A&A 592, A114 (2016)
DOI: 10.1051/0004-6361/201628650

Astronomy & Astrophysics

X-ray and optical observations of four polars⋆,⋆⋆

H. Worpel[1], A. D. Schwope[1], T. Granzer[1], K. Reinsch[2], R. Schwarz[1], and I. Traulsen[1]

[1] Leibniz-Institut für Astrophysik Potsdam (AIP), An der Sternwarte 16, 14482 Potsdam, Germany
e-mail: hworpel@aip.de
[2] Institut für Astrophysik, Friedrich-Hund-Platz 1, 37077 Göttingen, Germany

Received 6 April 2016 / Accepted 3 May 2016

ABSTRACT

Aims. We investigate the temporal and spectral behaviour of four polar cataclysmic variables from the infrared to X-ray regimes, refine our knowledge of the physical parameters of these systems at different accretion rates, and search for a possible excess of soft X-ray photons.

Methods. We obtained and analysed four *XMM-Newton* X-ray observations of three of the sources, two of them discovered with the SDSS and one in the RASS. The X-ray data were complemented by optical photometric and spectroscopic observations and, for two sources, archival *Swift* observations.

Results. SDSSJ032855.00+052254.2 was X-ray bright in two *XMM-Newton* and two *Swift* observations, and shows transitions from high and low accretion states on a timescale of a few months. The source shows no significant soft excess. We measured the magnetic field strength at the main accreting pole to be 39 MG and the inclination to be $45° \leq i \leq 77°$, and we refined the long-term ephemeris. SDSSJ133309.20+143706.9 was X-ray faint. We measured a faint phase X-ray flux and plasma temperature for this source, which seems to spend almost all of its time accreting at a low level. Its inclination is less than about 76°. 1RXSJ173006.4+033813 was X-ray bright in the *XMM-Newton* observation. Its spectrum contained a modest soft blackbody component, not luminous enough to be considered a significant soft excess. We inferred a magnetic field strength at the main accreting pole of 20 to 25 MG, and that the inclination is less than 77° and probably less than 63°. V808 Aur, also known as CSS081231:J071126+440405, was X-ray faint in the *Swift* observation, but there is nonetheless strong evidence for bright and faint phases in X-rays and perhaps in UV. Residual X-ray flux from the faint phase is difficult to explain by thermal emission from the white dwarf surface, or by accretion onto the second pole. We present a revised distance estimate of 250 pc.

Conclusions. The three systems we were able to study in detail appear to be normal polars with luminosities and magnetic field strengths typical for this class of accreting binary. None of the four systems studied shows the strong soft excess thought commonplace in polars prior to the *XMM-Newton* era.

Key words. white dwarfs – X-rays: binaries – binaries: close

1. Introduction

Polars are cataclysmic variable (CV) systems in which the white dwarf primary possesses a magnetic field strong enough to prevent the formation of an accretion disc. In these systems, material lost by the companion travels down magnetic field lines directly to an accreting pole of the white dwarf.

As the ionised gas spirals around the magnetic field lines it emits cyclotron radiation, which appears from infrared to ultraviolet wavelengths at the ∼10−230 MG field strengths in these systems. When the accreting material nears the white dwarf surface a shock forms and bremsstrahlung is emitted isotropically at X-ray wavelengths. Some of the bremsstrahlung is intercepted by the white dwarf surface and re-emitted as a blackbody-like feature in the extreme UV to soft X-ray range (e.g. Cropper 1990). Some polars exhibit accretion at both magnetic poles. For such systems, the pole more distant from the donor star typically has a stronger magnetic field but accretes less gas (e.g. Warner 1995; see also Table 2 of Ferrario et al. 2015, and references therein).

Many polars show an excess of energy in soft X-rays, far more than can be produced by re-emission of bremsstrahlung. This excess was initially hard to explain, but is now attributed to coherent blobs of gas penetrating deeply into the white dwarf atmosphere so that their energy escapes the white dwarf as a luminous blackbody-like component (e.g. Kuijpers & Pringle 1982; Ramsay & Cropper 2004). The soft excess led to many discoveries of polars with the *Einstein*, EXOSAT, ROSAT, and EUVE satellites and was suspected to be present in all polars. By the end of the ROSAT mission, over sixty soft excess polars were known (e.g. Thomas et al. 2000).

Every polar discovered in the *XMM-Newton* era, however, has lacked a large soft excess. Some of these new sources, such as V808 Aurigae (Worpel & Schwope 2015), are still bright enough in soft X-rays to have been detected in the ROSAT All-Sky Survey (i.e. they would have yielded at least six photons in the 0.1−2.4 keV band; Voges et al. 2000) but probably would have been too faint to be easily identified as polars. It is less clear why no new polars with the soft excess have been seen

⋆ Based on observations obtained with *XMM-Newton*, an ESA science mission with instruments and contributions directly funded by ESA Member States and NASA.

⋆⋆ Based on observations collected at the Centro Astronómico Hispano Alemán (CAHA) at Calar Alto, operated jointly by the Max Planck Institut für Astronomie and the Instituto de Astrofísica de Andalucía (CSIC).

in *XMM-Newton* data. Though this is a pointed rather than a survey instrument, it is capable of discovering them serendipitously (Vogel et al. 2008; Ramsay et al. 2009) and, while slewing, has a sensitivity comparable to ROSAT's (Saxton et al. 2008). Furthermore, several polars discovered optically in, for instance, the Sloan Digital Sky Survey (SDSS) have had follow-up *XMM-Newton* observations but have not shown a strong soft-excess. Our knowledge of the intrinsic shape of the spectral energy distribution of a typical polar is still clearly incomplete.

To further investigate this issue we analyse *XMM-Newton* data of three polar cataclysmic variables to look for possible soft excesses in these objects. The sources studied are summarised below. Additionally, we have optical photometric observations from the Catalina Real-Time Transient Survey (CRTS, Drake et al. 2009), the Sloan Digital Sky Survey (SDSS, Eisenstein et al. 2011), the STELLA robotic telescope (Strassmeier et al. 2004), and optical spectroscopy from Calar Alto. One source, SDSS J032855+052254.2, has previously unpublished archival *Swift* observations that we also present here.

In addition to seeking a soft X-ray excess, we aim to use the X-ray and optical data to find the rotation periods, system inclinations, and magnetic field strengths. These determinations contribute to a larger census of polars.

Finally, we present a previously unpublished *Swift* observation of the eclipsing polar V808 Aurigae in an X-ray faint state. The system was previously studied at high and intermediate luminosities (Schwope et al. 2015; Worpel & Schwope 2015). This work completes the characterisation of its X-ray and ultraviolet emission in all accretion states. We also present a revised distance estimate for this source.

SDSS J032855+052254.2, hereafter J0328, was identified as a polar in the SDSS. It is moderately optically bright, measured at g magnitude 18 in SDSS and varying between magnitudes 17 and 21 in CRTS. It shows evidence of cyclotron humps in its SDSS spectrum, and variability in its circular polarisation and Hα line velocity. The orbital period was determined to be 121.97±0.25 min by Szkody et al. (2007), who estimated a magnetic field strength of 33 MG at the accreting pole.

SDSS J133309.20+143706.9, hereafter J1333, is an optically faint source (about 18.5 g magnitude; Szkody et al. 2009) identified as a polar in SDSS. Its orbital period was measured to be 132 ± 6 min from radial velocity measurements of the Hα line (Schmidt et al. 2008). It shows optical brightness variations of about one magnitude at this period (Southworth et al. 2015).

1RXS J173006.4+033813, hereafter J1730, was detected as a moderately bright X-ray source (0.1 counts/s) in the ROSAT All-Sky Survey (Voges et al. 1999), and was also detected by *Swift* at about half this brightness in early 2006 (Shevchuk et al. 2009), but *Swift* observations in May 2009 showed that the source had dimmed to undetectability (Bhalerao et al. 2010). A 17th magnitude variable optical counterpart was discovered by Denisenko et al. (2009). Optical photometry and spectroscopy performed by Bhalerao et al. (2010) gives an orbital period of 120.2090 ± 0.0013 min, a magnetic field strength of ~42 MG, and an upper limit to the distance of 830 pc.

V808 Aurigae, previously known as CSS081231: J071126+440405, is a polar discovered in the Catalina Sky Survey (Drake et al. 2009; Denisenko & Korotkiy 2009; Templeton et al. 2009). It is an eclipsing system with a period of 117.18 min, eclipse duration 7.218 min, and an inclination of 79.3°−83.7° (Schwope et al. 2015). The companion star is probably an M4.6 red dwarf, as suggested by the period-secondary relations given in Knigge (2006). It has optical magnitudes $m_V \approx 21$ and $m_B \approx 22.4$ (Thorne et al. 2010) consistent with this identification from which its distance was estimated to be 390 pc (Worpel & Schwope 2015). The variable star designation V808 Aur was assigned in December 2015 (Kazarovets et al. 2015).

Table 1. Observation log of the X-ray observations.

Target	OBSID	Inst.	Date	Exp (s)
J0328*	0675230201	*XMM*	2012-Jan-27	2629
J0328	0675230701	*XMM*	2012-Feb-18	13 042
J0328	00045622001	*Swift*	2012-Mar-20	387
J0328	00045622002	*Swift*	2012-Jun-29	3120
J0328	00045622003	*Swift*	2012-Jul-03	617
J0328	00045622004	*Swift*	2012-Jul-16	1073
J1333†	0675230601	*XMM*	2012-01-26	–
J1333*	0675230501	*XMM*	2012-Jan-26	10 803
J1730	0675230301	*XMM*	2012-Feb-19	18 251
V808 Aur	00031326001	*Swift*	2009-Jan-08	7391

Notes. The lengths of the *Swift* and GTI-filtered *XMM-Newton* EPIC-*pn* XRT exposures are given. (*) These exposure times are much shorter than the on-target time due to high radiation- see Sects. 3.1.2 and 3.2.1. The associated OM exposures are longer. (†) This nominally 7 ks observation failed and was repeated later on the same day.

The source light curves show bright and faint phases in both optical and X-rays, indicative of an accreting pole moving in and out of view as the white dwarf primary rotates. The source was studied at high and intermediate accretion states by Worpel & Schwope (2015), who found that at high accretion rates the other magnetic pole accretes visibly in X-rays and optical. There is also a light curve dip, caused by the accretion stream passing in front of the main emitting spot, seen at optical wavelengths (Katysheva & Shugarov 2012) and in X-rays, but surprisingly not in the ultraviolet (Worpel & Schwope 2015). In that paper, the magnetic field strengths of the two accreting poles were measured to be 36 and 69 MG at the primary and secondary poles, and their positions are only 140° apart on the surface of the white dwarf. The location of the primary accretion spot was found to depend on accretion rate, moving by ≈20° from a trailing to a leading longitude between the intermediate and high states.

2. Data reduction and analysis

2.1. *XMM-Newton*

Four *XMM-Newton* observations of three of the four sources are available, summarised in Table 1. The EPIC cameras (Strüder et al. 2001; Turner et al. 2001) observed in full frame mode with the thin filter in all observations, and the Optical Monitor (OM, Mason et al. 2001) was operated in imaging and fast modes with the *UVW1* and *UVM2* filters, with effective wavelengths of 2910 Å and 2310 Å respectively (Kirsch et al. 2004). We have not used the Reflection Grating Spectrometer (den Herder et al. 2001) data due to poor signal-to-noise.

We reduced the raw data with the Science Analysis System (SAS), version 14.0.0. The EPIC-*pn* and EPIC-MOS data were processed with the standard *epchain* and *emchain* tasks to generate calibrated event lists, and *epreject* was run for EPIC-*pn* data. All timing data were corrected to the solar system barycentre with the SAS *barycen* task. The data from all three X-ray instruments were filtered to exclude photons with energies below 0.2 keV and above 15.0 keV. The OM fast mode data were reduced with the *omfchain* task, with a bin size of 300 s.

Our source extraction regions are circles centred on the source; their precise locations were determined with the SAS *edetectchain* task. The best extraction radii were found with the *eregionanalyse* task. These are in the range 14−36 arcseconds in radius. The background extraction regions are rectangles lying as near to the source as practical, located so that source and background regions suffer approximately the same charge transfer inefficiencies from photon registration to charge readout. A circular area 2.5 arcsec larger than the source extraction region was excluded from the background region. We produced X-ray light curves using the *epiclccorr* task.

We fit the spectra with version 12.9.0 k of Xspec (Arnaud 1996), and we fit the data from all three X-ray instruments simultaneously. To avoid giving too much weight to bins with few photons, we used Churazov weighting (Churazov et al. 1996). We fitted the data between 0.2 and 10 keV for the EPIC-*pn* instrument, and between 0.2 and 8.0 keV for the MOS cameras.

2.2. *Swift* observations

Four observations of J0328 and one of V808 Aur were taken by *Swift* (Table 1). We reduced these observations with the *xrtpipeline* task and extracted source photon event lists from a 20 pixel (47.1″) circular region surrounding the source. We judged the position of the source visually. The background region was a large nearby region containing no source. To maximise the photon numbers, we did not impose any energy cuts. In none of these observations were there enough source photons to obtain a useful spectrum. The photon arrival times were corrected to the solar system barycentre using the *barycorr* task in the FTOOLS package (Blackburn 1995).

We did not use data from the Burst Alert Telescope. J0328 was not visible in the UVOT data, but V808 Aur was clearly visible. For this source the UVOT data were reduced with the standard imaging mode data analysis pipeline described in the UVOT Software Guide[1] to produce properly calibrated, flat fielded, and exposure-corrected images. For each subexposure of the image file, source detection was performed with the *uvotdetect* task.

3. Results

3.1. J0328

3.1.1. CRTS and STELLA photometry

The CRTS database (DR2, Drake et al. 2009) lists 349 photometric observations of J0328 between MJD 53 644.41 and 56 592.30 (2005 October 01 to 2013 October 27). The source varied between a minimum brightness of 20.82 and a maximum of 17.13 (unfiltered, i.e. white-light photometry). Only a few measurements revealed a brightness fainter than 20 mag. A more typical faint level seems to occur around mag 19.5. The light curve in original time sequence is indicative of the occurrence of high and low states with a brightness increase of about 1−1.5 mag within an orbital cycle and long-term variability of similar amplitude.

We downloaded the CRTS data and transformed the MJD timings to barycentric Julian dates using code developed by Eastman et al. (2010) and provided via the web pages of the Ohio State University[2]. A period search using the analysis of variance method (Schwarzenberg-Czerny 1989) revealed one pronounced periodicity close to the expected value: P = (7324.00 ± 0.02) s, which will be regarded as the orbital period of the binary. The new period agrees with our STELLA results (see below) and those of Szkody et al. (2007) and is of sufficient accuracy to connect all observations presented in this paper without cycle count error. The accumulated uncertainty over the eight years of photometric CRTS observations, which covers almost 35 000 revolutions of the binary, is 0.1 phase units.

Table 2. Log of STELLA photometric observations of J0328 in 2012.

Date	Obs interval +2 455 000d	Filter	Exp (s)	No. of exp
Feb. 21	979.35442–979.49616	g	60	126
Feb. 22	980.35512–980.49345	g	60	123
Feb. 23	981.41883–981.49139	g	60	65

Time-resolved photometric observations with the WiFSIP instrument on the STELLA telescope (Strassmeier et al. 2004) were obtained during three nights in February 2012 through SDSS g and r filters always under stable photometric conditions. A log of the observations is given in Table 2.

The raw data were corrected for electronic bias and dark current and were flatfielded with pipeline scripts provided by the instrument developers (Granzer et al. 2001). Differential photometry was performed with respect to a nearby star at RA(2000) = 52.23305 degrees, Dec(2000) = 5.35920, with *ugriz* magnitudes of 17.44, 15.97, 15.36, 15.09, 14.97.

The light curves in g- and r-bands display an on/off morphology similar to that reported by Szkody et al. (2007) which was quite naturally explained due to the presence of an active pole. The amplitudes of the light curves were about 1.6 mag in the g-band and about 1.3 mag in the r-band and are shown in Fig. 1. The rise to the bright phase is more gradual than the fall into the faint phase. There is no indication of a second accretion region. The optical behaviour is thus qualitatively similar to the X-ray (see Fig. 2), except for the lack of unambiguous evidence for a dip in the bright phase.

The end of the bright phase observed by STELLA on 2012 February 21 marks the zero point of the long-term ephemeris. We have defined it to be the time of half light of the decline to the faint phase, occurring at barycentric Julian date BJD(TDB) = 2 455 979.46865(6) in barycentric dynamical time.

The long-term ephemeris of J0328 thus becomes

$$\mathrm{BJD(TDB)} = 2\,455\,979.46865(6) + E \times 0.0847685(2). \quad (1)$$

For this orbital period, the semi-empirical tables of Knigge (2006) indicate an M4.3 donor star of $0.177^{+0.023}_{-0.019}\ M_\odot$ assuming an uncertainty of 0.3 in the stellar type. That paper assumes a mean WD mass of 0.75 $M_\odot$ with an intrinsic scatter of 0.16 $M_\odot$, which we will adopt as the WD mass and its uncertainty for this calculation. Since there are no eclipses, the inclination is constrained to $i \lesssim 77°$ using the method of Chanan et al. (1976). We observe the obscuration of the accretion region by the accretion stream (see Sect. 3.1.2), so the colatitude β of the magnetic pole must be less than i. We estimate from Fig. 1 that the bright phase, when the accreting pole is in view, lasts for $\Delta\phi_B = 0.55 \pm 0.05$

[1] http://swift.gsfc.nasa.gov/analysis/UVOT_swguide_v2_2.pdf

[2] http://astroutils.astronomy.ohio-state.edu/time/utc2bjd.html

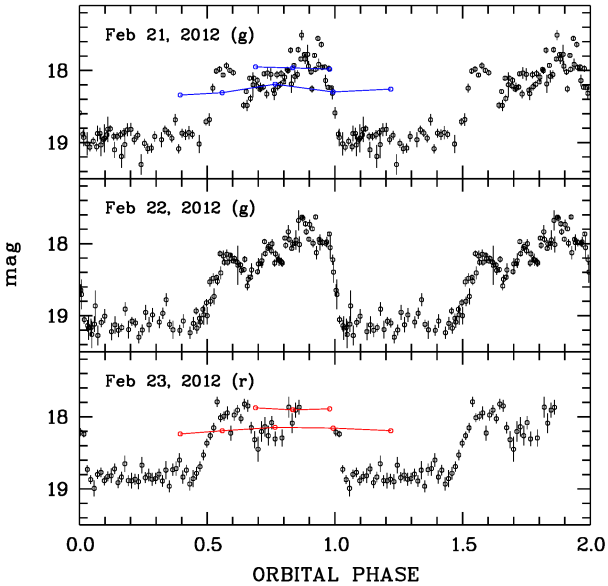

Fig. 1. STELLA/WiFSIP photometry of J0328. The data were folded using the period of 122.1 min. Coloured symbols connected by lines indicate SDSS-spectrophotometry.

of the binary orbit. From

$$\cot(i) = -\cos(2\pi\Delta\phi_B)\tan(\beta), \tag{2}$$

we solve for $i_{\rm min} = \beta$, assuming a spot with no vertical or lateral extent, to find the lower limit to the inclination, giving

$$i > \operatorname{arccot}\left[\sqrt{-\cos(2\pi\Delta\phi_B)}\right], \tag{3}$$

or $i \geq 45.0°$.

3.1.2. *XMM-Newton* X-ray observations

Two X-ray observations were made of this source, on 2012 January 27 and February 18. The light curves are shown in Fig. 2. The 2012 February 18 observation clearly shows distinct bright and faint phases characteristic of an emitting pole moving in and out of view. The bright phase is asymetrically shaped, with a slow rise to a maximum brightness of 0.6 counts/s and a more rapid decline. A deep dip in the bright phase is visible, lasting about seven min. This feature is likely due to the accretion stream passing in front of the pole. The faint phase has residual X-ray emission of about 0.1 counts/s, possibly emission from a second accretion region, but because there is no distinct second bump in the light curve this interpretation is uncertain. This observation is unaffected by proton flaring (Lumb et al. 2002), except for a short period of about 0.2 counts per second at the beginning of the observation. It does not affect our analysis at all, since it occurs during the faint phase.

According to the *XMM-Newton* observation logs the 2012 January 27 observation was affected by radiation, causing the EPIC-*pn* exposures to stop after 2629 s of the 26 ks on-target time, though the OM continued observing for considerably longer. Only around 470 s of data were recorded for the MOS instruments. In the remaining *pn* data the source is faint (~0.1 counts/s) but with an apparently rising intensity. According to our updated ephemeris (see Eq. (1)), this observation occurred around the beginning of the bright phase. As shown in Fig. 2, the source appears to have been slightly less luminous in both the bright and faint phases, perhaps indicating a reduced accretion rate, but this observation is too short to be certain. There

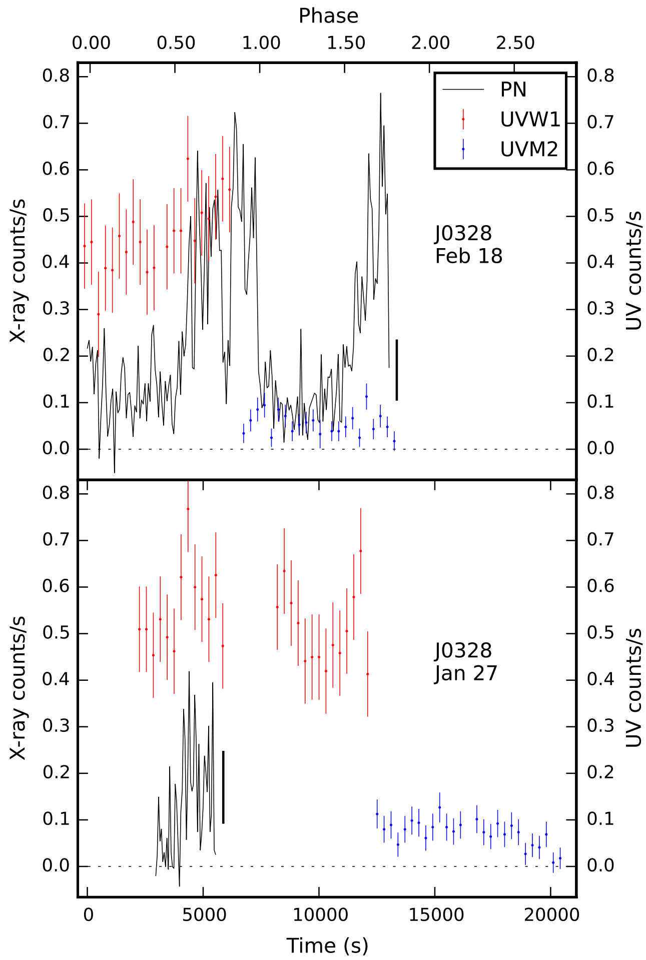

Fig. 2. EPIC-*pn* and OM light curves of J0328 for the 2012 January 27 and February 18 observations, in the 0.2–10.0 keV energy band. The bin size is 60 s for the X-rays and 300 s for the OM. The shorter exposure has been offset to the correct orbital phase according to the ephemeris given in Eq. (1). Mean uncertainties on the X-ray light curve is indicated by the thick vertical line to its right.

are not enough photons in this observation to obtain a useful bright phase spectrum. The remaining X-ray data in this observation was completely unaffected by proton flaring.

For the longer observation we extracted a bright phase spectrum, excluding the dip, for all three EPIC cameras. We fitted the spectra with a partially covered MEKAL plasma atmosphere model (Mewe et al. 1985; Liedahl et al. 1995), corrected for interstellar absorption with the *phabs* component, i.e. `phabs*pcfabs*mekal`. The plasma composition was left fixed at the solar value. We calculated errors to 99% significance on variable parameters using the *steppar* command. The results of these fits are given in Table 3, and the spectrum is shown in Fig. 3. For this source, the temperature of the plasma atmosphere was not strongly constrained. Since a pure plasma emission model suffices to describe the data, there is no need to add any other radiation component.

3.1.3. *XMM-Newton* optical monitor observations

The OM light curves are shown in Fig. 2. The source is faint and the quality is poor, but in the *UVW1* filter there are distinct indications of bright and faint phases corresponding to those seen in X-rays. The source is detectable, though very faint, in *UVM2* and

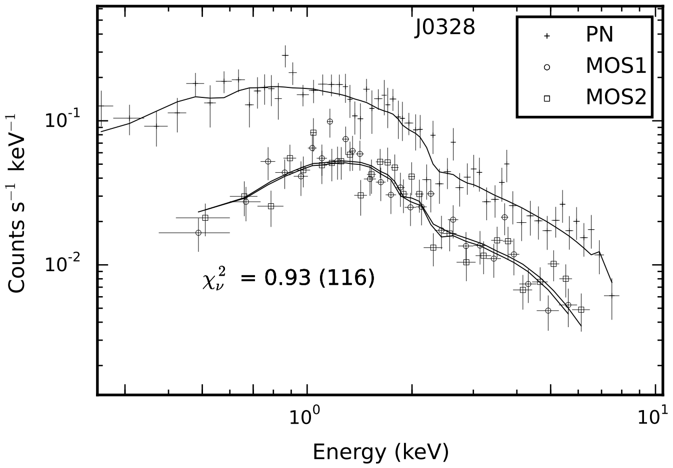

Fig. 3. Bright phase X-ray spectrum of J0328. The data were fit for the three EPIC instruments simultaneously with a MEKAL plasma atmosphere model with both local and interstellar absorption.

Table 3. Spectral fits to the bright phase spectra of J0328.

	J0328
Interstellar N_H (10^{20} cm^{-2})	$8.7^{+2.9}_{-1.9}$
pcfabs N_H (10^{22} cm^{-2})	16^{+60}_{-11}
covering fraction	$0.27^{+0.05}_{-0.05}$
$kT_{\rm mekal}$ (keV)	15
norm$_{\rm mekal}$	$1.2^{+0.1}_{-0.1}$
Flux$_{\rm mekal,unabs}$ (10^{-12} erg s^{-1} cm^{-2})	$3.1^{+0.2}_{-0.2}$
Flux$_{\rm mekal,abs}$ (10^{-12} erg s^{-1} cm^{-2})	$2.3^{+0.2}_{-0.1}$
χ^2_ν (d.o.f.)	0.95 (115)
Flux$_{(0.1-2.4),\rm abs}$ (10^{-13} erg s^{-1} cm^{-2})	$5.0^{+0.3}_{-0.3}$

Notes. Normalisations for the MEKAL model are given in units of $10^{-17}\int n_e n_H dV/4\pi[D_A(1+z)]^2$, where D_A is the angular diameter of the source, and n_H, n_a are the hydrogen and electron densities. Normalisations for the blackbody model are in units of $(R/D_{10})^2$ where R is the radius of the object in kilometers and D_{10} is its distance in units of 10 kpc. We give both absorbed and unabsorbed plasma atmosphere fluxes and in the last row we give the absorbed flux in the ROSAT band. We note that the temperature is fixed at 15 keV.

shows no evidence of phase modulation. The top panel clearly shows that the bright phase dip seen in X-rays is not present in the UV.

It is conceivable that a large soft excess might be present in the extreme UV/very soft X-ray regime. We estimated the largest unobserved blackbody in a manner very similar to the approach in Worpel & Schwope (2015). As reasoned in that paper, the unobserved soft excess can come from a region no larger than the white dwarf surface (which we assume to be $R_{bb} < 8000$ km), its temperature can be no lower than that of the coolest known polar primary (0.64 eV; Schmidt et al. 2005; Ferrario et al. 2015), its presence should not affect the observed X-ray spectrum, and it should not overpredict the UV flux arising from the accretion region in either the *UVW1* or *UVM2* filters.

We simulated a series of blackbodies, whose temperatures and normalisations were on a grid with 0.5 eV $< T_{bb} <$ 50 eV and 1 km $< R_{bb} <$ 8000 km. The blackbody effective radii are expressed as the radii of a sphere at the distance of J0328. The

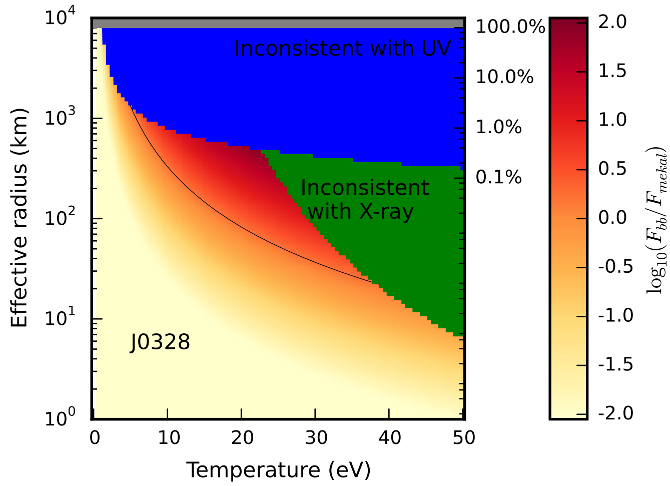

Fig. 4. Parameter space in which a soft excess can exist for J0328. The green regions indicate areas excluded because they conflict with the *XMM-Newton* X-ray observations, the blue region indicates areas ruled out because they overpredict the UVW1 energy density, and the grey region indicates an emitting area larger than the surface of the assumed 8000 km radius WD. The shaded region indicates the magnitude of the potential soft excess (i.e. its flux divided by that of the X-ray plasma component). The black curve tracks where these are equal, indicating what would be expected for a bremsstrahlung being half intercepted and re-radiated. The right y-axis expresses the emitting area as a percentage of the WD surface.

distance of J0328 is unknown, but we estimate it as follows. We assume that at most 5% of the flux of the system between 7440 and 7520Å comes from the companion star. This scaling gives m_R = 19.44. Assuming a mass for the primary of 0.75 $M_\odot$, a spectral type for the companion of M4.0 to M4.6, and an inclination of 60° (see Sect. 3.1.1) we obtain effective radii for these stellar types by numerically computing the projected Roche lobe geometry for a range of orbital phases. Equations (7) and (8) and Table 2 of Beuermann (2006) give a distance lower limit of 250 pc.

This lower limit is less constraining than the recent work of Coppejans et al. (2016), who give a minimum distance of 559 pc. We point out that such a large distance appears unlikely because of J0328's high Galactic latitude (b = −40°). A distance of 559 pc puts the source 360 pc below the Galactic plane or 1.6−4.3 scale heights for the Galactic CV population (Revnivtsev et al. 2008). We therefore adopted a conservative distance estimate of 500 pc for the exercise of constraining the possible hidden soft excess. We then fitted the spectra between 200 and 1000 eV with the sum of the trial blackbody and the plasma atmosphere model of Table 3. Trials that caused the χ^2_ν to increase by more than 1 were rejected. We also rejected trials that overpredicted the accretion region flux density in either UV band, defined as the average bright phase flux density minus the average faint phase flux density, plus the propagated 1σ uncertainty (see Fig. 2). The mean bright phase UV flux densities were formally (6.7 ± 6.8) × 10^{-5} keV cm^{-2} s^{-1} and (−0.6±2.7)×10^{-5} keV cm^{-2} s^{-1} for the *UVW1* and *UVM2* filters, i.e. both consistent with zero.

The bolometric flux of the potential soft blackbody was then compared to the flux of the plasma atmosphere model. The results are shown in Fig. 4. The largest soft excess formally compatible with the observations is 88 times as luminous as the plasma component for a 22.5 eV blackbody with an effective radius of 460 km. It is near to being ruled out by both the X-ray and

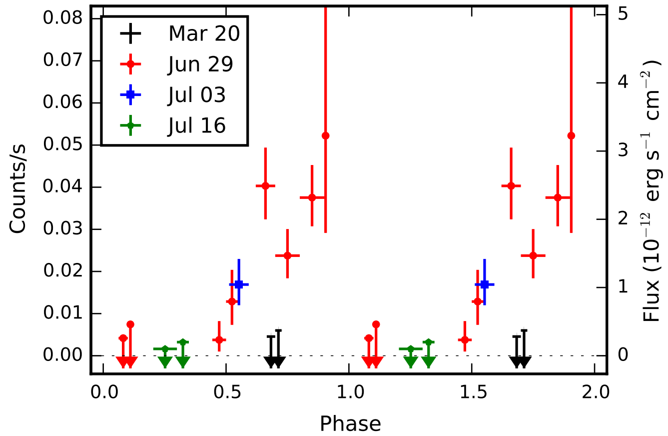

Fig. 5. Phase-folded light curves of the four *Swift* observations of J0328, obtained between March and July 2012. Two cycles are shown for clarity. Points with no source counts have upper detection limits indicated by arrows. The right axis indicates the flux in the *XMM-Newton* band assuming the bright phase spectrum listed in Table 3.

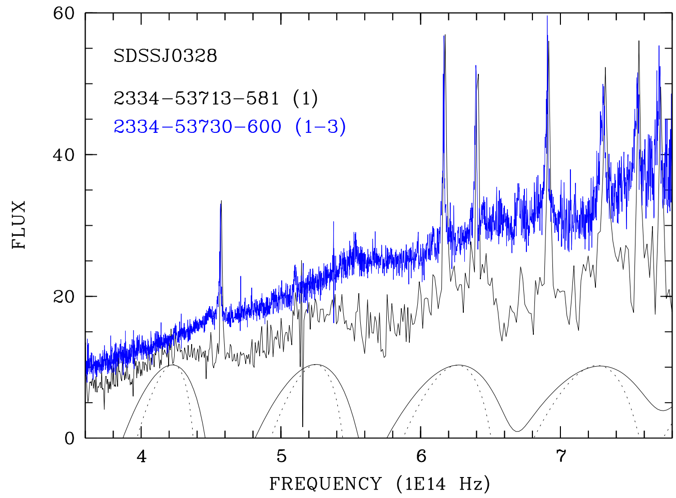

Fig. 6. SDSS spectra of J0328. Labels identify plate, MJD, fibre number and the subspectrum. The single 15 min spectrum obtained MJD 53 713 was median filtered for display purposes. Below the spectra cyclotron absorption coefficients originating from a 5 keV plasma are shown (see text for details). The units of flux are 10^{-17} erg s^{-1} cm^{-2} Å^{-1}.

UV data, and it is likely that more sensitive observations could have excluded it. Nevertheless it is possible that a substantial excess of flux can be concealed in the very soft X-ray range. If J0328 were nearer or further than 500 pc, then the boundaries of the green and blue regions would move down or up respectively.

3.1.4. *Swift* X-ray observations

The source was detectable only in the 2012 June 29 and July 3 observations, with a total of 81 and 10 photons. Phase-folded light curves, according to the ephemeris in Eq. (1), are shown in Fig. 5. Though the phase coverage is not complete, the bright and faint phases are evident in the longer observation.

The 2012 March 20 observation occurred during the bright phase. Its non-detection suggests that J0328 was in a lower accretion state at that time. It is too early in phase to coincide with the accretion dip. If we conservatively assume that we require six photons to detect the source, we get an upper limit of 0.016 counts/s, less than half the brightness of the June 29 observation at the same phase.

The 2012 July 16 observation occurred during the faint phase, so the non-detection of the source is unsurprising. The upper limit on the count rate is 0.0056 counts/s for six counts in a 1073 s observation.

The short 2012 July 3 observation occurs during the rise to the bright phase. It closely matches the corresponding points in the longer June 29 observation, suggesting that the accretion rate did not change much in the few days between those pointings.

We found the 1σ uncertainties on the background subtracted counts, following Kraft et al. (1991), by integrating over the Poisson probability distributions, except that we also take into account the uncertainties in background rate as outlined in Helene (1983), Eq. (5).

There are not enough photons in any *Swift* observation to extract spectra, but – assuming the same spectral shape as the February 18 *XMM-Newton* observation – a *Swift* count rate of 0.01 counts per second corresponds to a flux in the 0.2−10 keV EPIC-*pn* band of 6.2×10^{-13} erg s^{-1} cm^{-2}. This suffices as a rough cross-calibration between the two sets of observations. The source has returned to approximately its February 2012 brightness ($\sim 2 \times 10^{-12}$ erg s^{-1} cm^{-2} in the bright phase) by late June.

3.1.5. SDSS spectroscopy

The SDSS (Eisenstein et al. 2011) observed J0328 spectroscopically two times using the same plate (plate number 2334). The first observation happened through fibre 581 on MJD 53 713, the second on MJD 53 730 through fibre 600. These observations will henceforth be designated 2334-53 713-581 and 2334-53 730-600 (i.e. plate-mjd-fibre). The first observation consists of five subspectra of 15 min each covering binary cycles −26 728.6 to −26 727.8. The second observation had three subspectra covering binary cycle −26 529.3 to −26 529.0. Undulations of the continuum reminiscent of cyclotron harmonics were reported by Szkody et al. (2007) from follow-up spectroscopy of the source.

In order to gain further insight into the behaviour of the cyclotron features we inspected all the subspectra. It turned out that the cyclotron features were found to be most obvious in the first subspectrum of 2334-53 713-581. This subspectrum and the yet unpublished average second spectrum are shown in Fig. 6. Cyclotron humps appear at about 4.2, 5.2, and 6.3×10^{14} Hz in 2334-53713-581 revealing a field strength of about 38 MG.

The observed spectra are shown together with the cyclotron absorption coefficient for a 5 keV plasma at 38.5 MG (viewing angle 70°) and 39 MG (viewing angle 80°) which was normalised to a smooth continuum beforehand. There is 1 MG uncertainty due to the unknown viewing geometry, and another 1 MG uncertainty that stems from the unknown plasma temperature. Our revised field strength is 39 ± 2 MG. The field strength of 33 MG derived by Szkody et al. (2007) identifies the hump at 5.2×10^{14} Hz with the 6th harmonic instead of the 5th and leads to a non-matching lower harmonic.

At the epoch of the second observation, 2334-53 730-600, the object was brighter and the continuum was less modulated by cyclotron emission. The three subspectra cover the phase interval 0.7−1.0 in cycle −26 529. There appears to be a single hump at 5.5×10^{14} Hz. A single feature, however, is not sufficient to determine a field strength.

Synthetic SDSS-magnitudes were computed for each subspectrum by folding the spectral data through instrumental filter curves. The resulting light curves are also shown in Fig. 1. On both occasions when the bright phase was observed, the

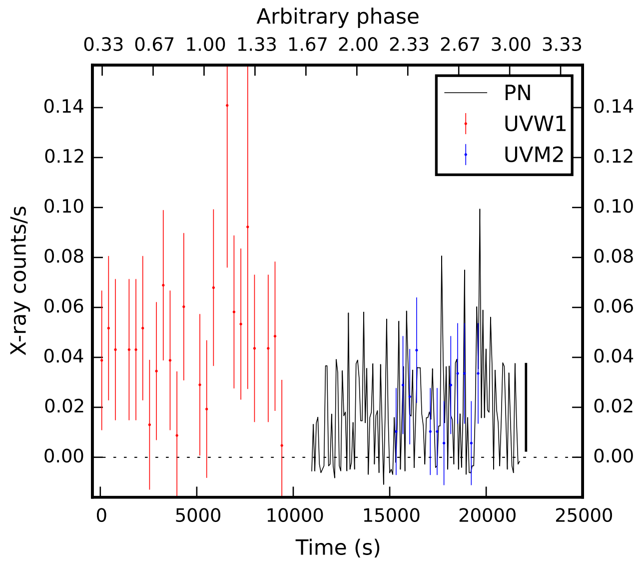

Fig. 7. EPIC-*pn* and OM light curves of J1333 for the 2012 January 26 observation, in the 0.2–10.0 keV energy band. The bin size for X-rays is 60 s, and 300 for UV. Mean uncertainties on the X-ray data are indicated by the thick error bar to its right.

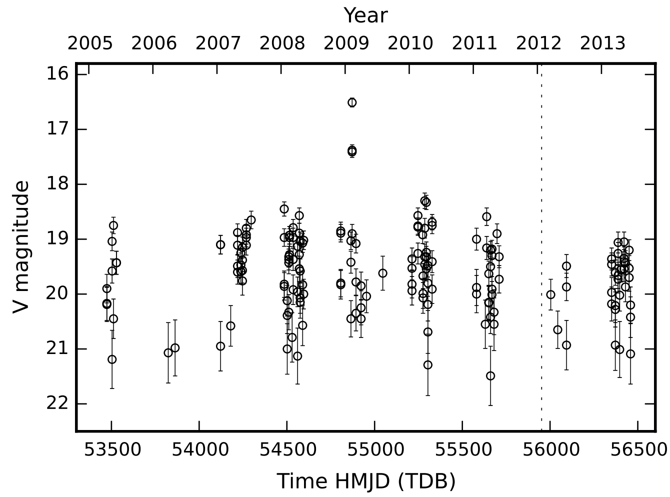

Fig. 8. CRTS light curve of J1333. The system remains between magnitudes 18.3 and 21.5, except for a brief brightening in early 2009. The time of the *XMM-Newton* observation is indicated with a vertical dashed line.

photometric variability was much lower than expected from our own and published photometry (Szkody et al. 2007), indicating a remarkable change in the accretion geometry of the source.

An estimate of the cyclotron flux of J0328 was derived by assuming that the excess radiation forming the optical bright phase is pure cyclotron radiation with a spectral shape given by the SDSS spectrum 2334-53 730-600. This results in an observed integrated cyclotron flux of $F_{\rm cyc} = 6.3 \times 10^{-13}$ erg s^{-1} cm^{-2}. The cyclotron spectrum peaks in the unobserved ultraviolet and is expected to fall off rather quickly in the optically thin regime at even shorter wavelengths. We estimate a bolometric correction factor of 1.3; this gives $F_{\rm cyc,bol} = 8.2 \times 10^{-13}$ erg s^{-1} cm^{-2}, which is lower by a factor 3 than the plasma X-ray emission. Cyclotron cooling seems to play a minor role in this high accretion state despite the rather large field strength.

3.2. J1333

3.2.1. *XMM-Newton* observations

This source was observed by *XMM-Newton* on 2012 January 26. Owing to high radiation levels, *XMM-Newton* only recorded for about 11 ks of the 22 ks on-target time, but the remaining X-ray data in this observation were completely unaffected by proton flaring. The X-ray light curve is shown in Fig. 7. It is clear that the source was in a low accretion state during the *XMM-Newton* observation, and that distinguishing bright and faint phases is impossible. The source was detectable using the SAS *edetectchain* task, and we extracted a very low resolution *pn* X-ray spectrum. We fitted this spectrum with a MEKAL model between 0.2 and 8 keV, giving a χ^2_ν of 0.72 for 19 degrees of freedom, and the average flux over the observation was 2.75×10^{-14} erg s^{-1} cm^{-2}. The inferred plasma temperature was low, about 4.3 keV. The spectrum could be fitted just as well using a bremsstrahlung spectrum or an absorbed power law but the measured flux in the 0.2 to 8 keV band did not change significantly by changing the spectral model. The source was not bright enough for us to investigate any possible soft excess, or to look for any periodicity.

3.2.2. *XMM-Newton* optical monitor observations

The source was very faint (Fig. 7), with count rates of 0.048 ± 0.028 and 0.022 ± 0.013 counts per second in the *UVW1* and *UVM2* bands. According to the conversion factors of Kirsch et al. (2004) these count rates are equivalent to $(2.1 \pm 1.2) \times 10^{-17}$ erg s^{-1} cm^{-2} Å^{-1} and $(4.7 \pm 2.5) \times 10^{-17}$ erg s^{-1} cm^{-2} Å^{-1} for the *UVW1* and *UVM2* filters, respectively. There is no evidence for bright and faint phases.

3.2.3. CRTS photometry

The CRTS database (DR2, Drake et al. 2009) lists 171 photometric observations of J1333 between MJD 53 469.35 and 56 454.26 (2005 April 9 to 2013 June 11). The source varied between a minimum brightness of 21.49 and a maximum of 18.30 (unfiltered, i.e. white-light photometry), except for a brief increase in brightness to 16.51 on 2009 February 5 (see Fig. 8). We performed barycentric corrections and a period search as in Sect. 3.1.1 around the inferred orbital period of 132 min (Schmidt et al. 2008) but no periodicities were detected.

There is no evidence for eclipses in our *XMM-Newton* data, the CRTS light curves, or the light curves presented in Schmidt et al. (2008) and Southworth et al. (2015). The inclination is therefore less than about 76°, following the arguments in Sect. 3.1.1. The orbital period of 2.2 h places this system in the orbital period gap, where the tables of Knigge (2006) are incomplete, but the companion masses either side of the period gap are about 0.2 $M_\odot$, slightly more massive than the companion in J0328, so we used 0.2 $M_\odot$ for the above calculation.

3.3. J1730

3.3.1. *XMM-Newton* observations

This source was observed by *XMM-Newton* on 2012 February 19. The X-ray light curve is given in Fig. 9. This light curve is typical of polars, showing a radiating pole rotating in and out of view. Approximately 2.5 orbital periods were covered by *XMM-Newton* and are shown in the figure.

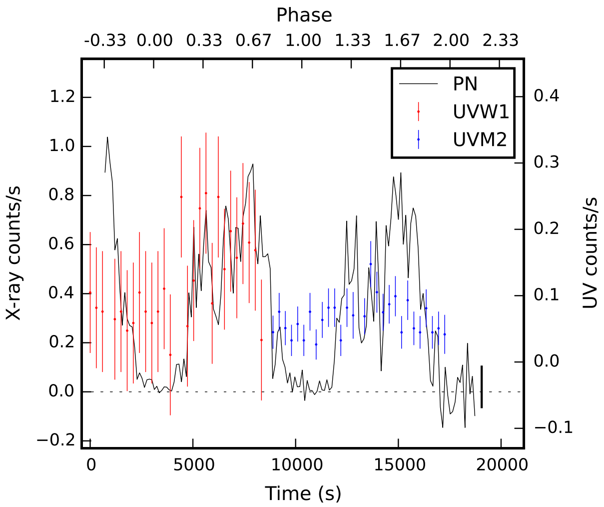

Fig. 9. EPIC-*pn* and OM light curves of J1730 for the 2012 February 19 observation, in the 0.2–10.0 keV energy band. The bin size is 120 s for X-rays and 300 s for UV. The mean uncertainty on the X-ray light curve is indicated by the thick error bar to the right. Phases are calculated according to the ephemeris of Eq. (4).

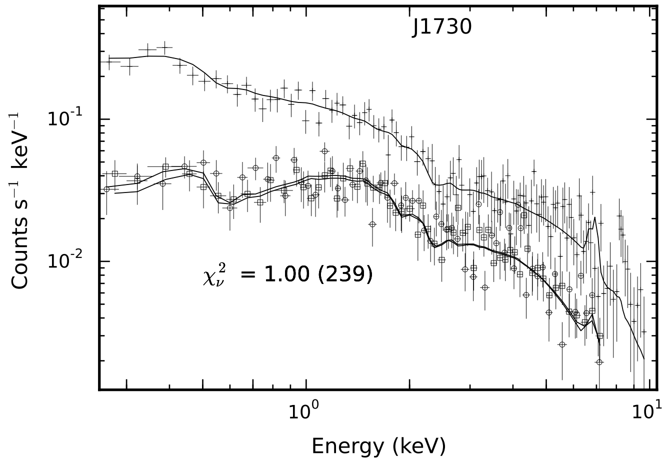

Fig. 10. Bright phase X-ray spectrum of J1730 fitted for the three EPIC instruments simultaneously with a MEKAL plasma atmosphere model and a large soft blackbody, corrected for both local and interstellar absorption.

The bright phases reach a peak brightness of ~1 count s^{-1}. The first half of the second cycle shows rapid, intense variability. There may be an accretion dip feature at around phase 0.33, but because of the variability in the light curve immediately before and after it, the evidence for a dip is not as clear as it was for J0328. There is no residual X-ray emission in the faint phase, and hence no evidence for a second accretion region.

We extracted a bright phase spectrum for this source as we did for J0328. Fitting the J1730 data required some care. Using just a plasma atmosphere left large residuals at both the high and low energy ends of the spectrum. We therefore had to use both a partially covering absorber to prevent implausibly high plasma temperatures and a cool blackbody to account for an excess of soft photons. We then modelled the spectra with the sum of a soft blackbody and a warmer MEKAL plasma atmosphere, both absorbed by a partially covering photoelectric absorber and interstellar absorption: `wabs*pcfabs*(bbodyrad+mekal)` in Xspec. We imposed an upper limit of 7.0×10^{20} cm^{-1} for the interstellar absorption, the column density in the direction of J1730 (Denisenko et al. 2009). We found that a slight excess of high energy (>5.0 keV) photons causes the MEKAL component to reach unphysically high temperatures. Thus, we fixed the plasma temperature at 15 keV. The spectrum is shown in Fig. 10 and the fit parameters are given in Table 4. Changing the fixed plasma temperature to 10 or 20 keV does not significantly change the flux of this component or of the blackbody.

We calculated the unabsorbed bolometric fluxes of the plasma and blackbody components between 10^{-6} and 100 keV using Xspec's *cflux* tool. The chosen energy range is wide enough that small changes to the upper and lower limits do not affect the result. The component fluxes are also listed in the table. The soft blackbody is two to three times less luminous than the plasma emission, and may therefore represent part of the expected and sought-after reprocessed component but there is no evidence for a significant soft excess for this source either.

The field is not covered by CSS, hence no further long-term photometry except for that from Bhalerao et al. (2010) is available to compare the new *XMM-Newton* data with.

The bright phase for this source is longer than for J0328. The orbital period implies an M4.4 donor of 0.171 $M_\odot$ and 0.208 $R_\odot$.

Table 4. Spectral fits to the bright phase spectra of J1730.

	J1730
Interstellar N_H (10^{20} cm^{-2})	$5.0^{+2.0}_{-4.1}$
pcfabs N_H (10^{22} cm^{-2})	$6.4^{+7.1}_{-3.4}$
covering fraction	$0.52^{+0.08}_{-0.09}$
kT_{bb} (eV)	59^{+18}_{-12}
norm$_{bb}$	$13{,}000^{+86{,}000}_{-12{,}000}$
$kT_{\rm mekal}$ (keV)	15
norm$_{\rm mekal}$	$1.5^{+0.2}_{-0.2}$
Flux$_{\rm bb}$ (10^{-12} erg s^{-1} cm^{-2})	$1.7^{+0.3}_{-0.3}$
Flux$_{\rm mekal}$ (10^{-12} erg s^{-1} cm^{-2})	$3.9^{+0.2}_{-0.2}$
χ^2_ν (d.o.f.)	1.00 (239)
Flux$_{(0.1-2.4)}$ (10^{-13} erg s^{-1} cm^{-2})	$5.8^{+0.3}_{-0.2}$

Notes. Normalisations for the MEKAL model are given in units of $10^{-17} \int n_e n_H dV/4\pi[D_A(1+z)]^2$, where D_A is the angular diameter of the source, and n_H, n_a are the hydrogen and electron densities. Normalisations for the blackbody model are in units of $(R/D_{10})^2$ where R is the radius of the object in kilometers and D_{10} is its distance in units of 10 kpc. Spectral component fluxes are unabsorbed bolometric fluxes. In the last row we give the absorbed flux in the ROSAT band. We note that the plasma temperature is fixed at 15 keV.

We estimate $\Delta\phi_B \approx 0.6 \pm 0.1$. Following the same reasoning as in Sect. 3.1.1 the apparent absence of an accretion dip suggests that $i \lesssim 63°$ because the inclination in this case must be less than the colatitude of the accretion spot. However, the intense variability of the first half of the bright phase means that we cannot place much weight on this interpretation. The lack of eclipses definitely constrains the inclination to $i \lesssim 77°$, following the same procedure as in Sect. 3.1.1.

3.3.2. *XMM-Newton* optical monitor observations

The OM light curve is shown in Fig. 9. The source is faint, with a maximum count rate of about 0.2 count s^{-1} for the *UVW1* filter. It appears that the bright phase is visible in the *UVW1* data,

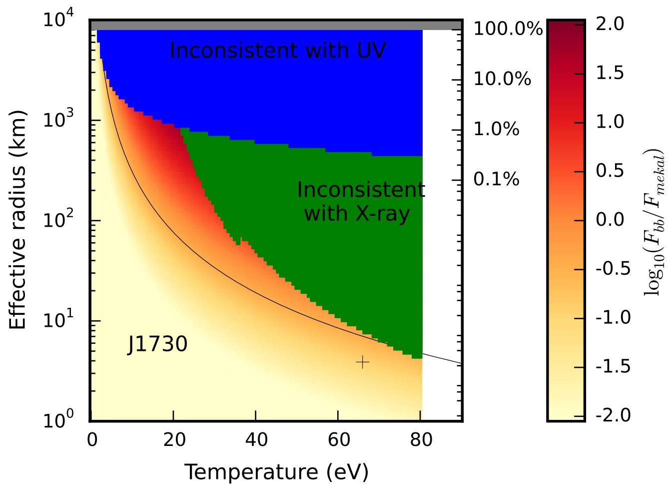

Fig. 11. Parameter space in which a soft excess can exist for J1730. The green regions indicate areas excluded because they conflict with the *XMM-Newton* X-ray observations, the blue region indicates areas ruled out because they overpredict the *UVW1* energy density, and the grey region indicates an emitting area larger than the surface of the assumed 8000 km radius WD. The shaded region indicates the magnitude of the potential soft excess (i.e. its flux divided by that of the X-ray plasma component). The black curve tracks where these are equal, indicating what would be expected for a bremsstrahlung being half intercepted and re-radiated. The right y-axis expresses the emitting area as a percentage of the WD surface. The black cross shows the location of the soft blackbody we actually detected in this spectrum, and the diamond indicates the most luminous blackbody for a nearer (560 pc) distance.

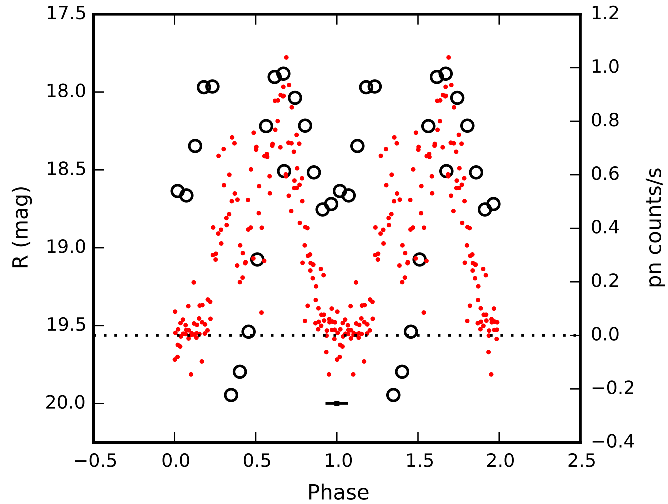

Fig. 12. Approximate Johnson R-band light curves derived from time-resolved spectrophotometric observations of J1730 on August 13, 2013 (large circles) and phase-folded EPIC-*pn* count rates (small points). The cycle is plotted twice for clarity. The horizontal error bar indicates the maximum accumulated phase uncertainty between the optical and X-ray observations. The dotted horizontal line indicates zero *pn* count rate.

and that it decreases to the faint phase before the X-rays do. Because of the faintness of the source, it is not possible to tell whether the bright phase dip visible in X-rays is present in UV. The flux densities of the accreting pole emission, defined as the mean flux density of the bright phase minus that of the faint phase, were $(2.1 \pm 2.4) \times 10^{-4}$ keV cm^{-2} s^{-1} and $(0.3 \pm 1.0) \times 10^{-4}$ keV cm^{-2} s^{-1} for the *UVW1* and *UVM2* filters.

We estimated the largest possible soft blackbody flux in a similar manner to 3.1.2, except that the assumed distance is 830 pc and we substitute the grid soft blackbody for the one in the existing spectrum rather than adding a completely new component. The results of this analysis are given in Fig. 11. The maximum temperature is 80 eV (roughly, the measured value plus the upper uncertainty; see Table 4). For this source the largest possible unobserved blackbody (T_{bb} = 18.5 eV, R_{bb} = 980 km) is 65 times as luminous as the plasma component, again for an emission region that covers a large area of the white dwarf surface and is only barely consistent with the X-ray, *UVW1*, and *UVM2* data. The 830 pc distance is an upper limit; smaller distances would move the blue and green regions downward and exclude these large soft blackbodies. For instance, applying Eq. (3) of Bhalerao et al. (2010) to the companion radius predicted for J1730's orbital period in Knigge (2006), we obtain an estimated distance of 560 pc. The most luminous hidden soft blackbody for this distance is indicated with a diamond in this figure. The discontinuity in the green curve is a point at which the flux at the low energy end is no longer underpredicted, but the χ^2_ν is not too high for an acceptable fit.

3.3.3. Calar Alto spectroscopy

Low-resolution spectroscopy of J1730 was performed during the night of 2013 August 13 with the 2.2 m telescope of the Calar Alto observatory. The telescope was equipped with CAFOS, a low-resolution grism spectrograph and imager. The G200 grism provided wavelength coverage from 3750 Å to 1.05 μm (useful range below 9200 Å) at a FWHM resolution of about 12 Å through a 1.2 arcsec slit, as measured from calibration lamp spectra. The integration time per spectrum was 5 m. A total of 18 spectra, covering slightly more than one orbital period, were taken. The airmass varied from 1.23 to 1.65 over the series of exposures.

The spectrograph was rotated so that the light of the two stars USNO-B1.0 0936-00303765 (RA = 17:30:02.78, DE = +03:38:32.8, B = 17.0, R = 15.8) and USNO-B1.0 0936-00303745 (RA = 17:30:01.48, DE = +03:38:37.7, B = 16.1, R = 15.5) was also falling through the slit and could be used for the correction of slit losses of the target star.

Arc lamp spectra (Hg+He+Rb) for wavelength calibration and standard stars for photometric calibration were obtained before and after the sequence of the target star. Standard star spectra were obtained through wide and narrow slits. While the spectra that were obtained through wide slits were used to determine the shape of the instrumental response curves, the one obtained through the narrow slit was used for scaling purposes.

An approximate Johnson R-band light curve was extracted from the time-resolved photometric spectra using the ESO-MIDAS software (Warmels 1992), and is shown in Fig. 12. The overall brightness and the light curve shape indicate that J1730 was observed in an active state, similar to epochs #1 and #4 of Bhalerao et al. (2010). The large amplitude modulation of the light curve is reminiscent of that shown by MR Ser or V834 Cen in their high accretion states. In those sources the optical light curves were modulated by strong cyclotron beaming.

We use the ephemeris defined by Bhalerao et al. (2010):

$$\mathrm{BJD(TDB)} = 2\,454\,988.9375(3) + E \times 0.0834785(9). \qquad (4)$$

The *XMM-Newton* and Calar Alto observations are 6483 cycles apart, and the uncertainty in the period introduces an error of less than 0.006 in phase units. This is precise enough to put the Calar Alto and *XMM-Newton* light curves on a common scale.

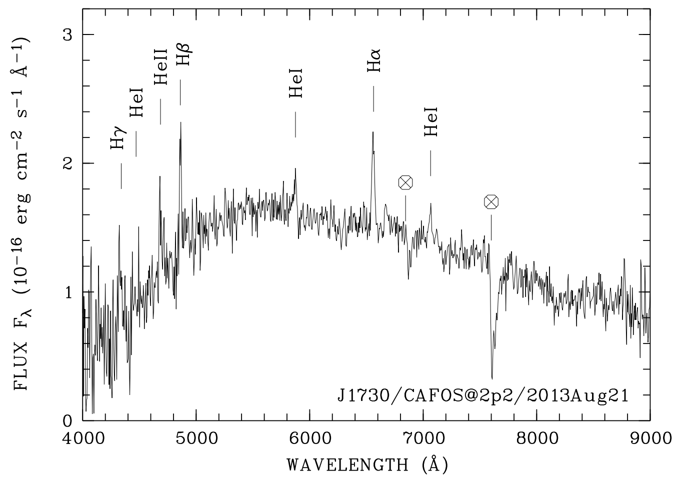

Fig. 13. Average mean bright spectrum of J1730 obtained 2013 August 21. Main emission lines and uncorrected telluric absorption features are labelled.

An average spectrum of the four brightest individual spectra is shown in Fig. 13. Apart from H-Balmer, HeI and HeII emission lines that are typical for polars in their high accretion states the spectrum is dominated by a prominent continuum component which peaks at roughly 5500 Å. It drops to ~40% of its peak value at 4000 Å. The decrease towards the red spectral regime is more moderate. This continuum spectral component is naturally explained as cyclotron radiation and the wavelength of the peak spectral flux indicates the turn-over of optically thick radiation at long wavelength to thin radiation at short wavelength/high harmonic number due to the strong frequency dependence of the cyclotron absorption coefficient. In a high state polar, the peak harmonic number is typically around 8 which gives a field estimate of around 25 MG. Objects with similar field strength in their main accretion regions are MR Ser and V834 Cen which show similar shapes of their high-state cyclotron continua (Schwope et al. 1993; Schwope & Beuermann 1990). We note in particular that a field strength of 42 MG deduced by Bhalerao et al. (2010) cannot be confirmed by our observations. Our data would cover the harmonic range 3−6 and it would likely have been possible to resolve individual cyclotron harmonics in this low harmonic regime.

The integrated cyclotron flux at maximum phase is 7×10^{-13} erg s^{-1} cm^{-2}. The bolometric correction is an estimated 15% so that the total flux at maximum phase becomes 8×10^{-13} erg s^{-1} cm^{-2}. The cyclotron flux is therefore fainter than the bremsstrahlung flux by a factor of around five (see Table 4). Taking into account that the cyclotron emission is beamed and that the bremsstrahlung is re-radiated from the WD surface, their combined luminosity is

$$L = \pi d^2 \left(2F_{\rm brems} + \frac{3}{2} F_{\rm cyc} + 2F_{\rm bb} \right). \tag{5}$$

From the upper distance limit of 830 pc (Bhalerao et al. 2010) we conclude that the total luminosity is less than 2.6×10^{32} erg s^{-1}.

3.4. V808 Aur (CSS081231:J071126+440405)

Worpel & Schwope (2015) provided a first estimate of the distance of 390 kpc. A more sophisticated estimate using the method of Beuermann (2006) gives a nearer distance of about 250^{+50}_{-40} pc.

Table 5. Five UVOT subexposures.

Exp	Flux	$t_{\rm bri}$	$t_{\rm fai}$	$t_{\rm ecl}$	$t_{\rm tot}$	Phase
1	1.33	–	1493.2	–	1493.2	0.34-0.56
2	1.29	794.4	696.7	–	1491.1	0.17-0.38
3	1.29	1213.1	–	280.9	1494.0	0.99-0.20
4	1.31	985.6	–	433.1	1418.7	0.83-0.03
5	1.47	459.4	1034.9	–	1494.3	0.64-0.85

Notes. Fluxes in the *UVOT-UVW2* band are given in units of 10^{-15} erg s^{-1} cm^{-2} Å^{-1}. For each measurement the uncertainty is 3×10^{-17} erg s^{-1} cm^{-2} Å^{-1}. Times in seconds are given for the bright, faint, and eclipse phases, and for their sum.

3.4.1. *Swift* X-ray observations

The XRT (Burrows et al. 2005) detected V808 Aur emitting very weakly, with 26 source region photons over the 7.4 ks observation, from a circular extraction region of 20 pixels (47.1″). The background intensity was 4.5×10^{-3} counts per pixel, based on a large region containing no source, so there are probably five or six background photons in the source extraction region. This equates to a source count rate of $2.8 \pm 0.7 \times 10^{-3}$ counts per second. There are clearly too few photons to extract a spectrum, or to produce a meaningful light curve.

The 26 source region photons were divided into nominally bright and faint phase categories according to the ephemeris given in Schwope et al. (2015) and assuming a leading spot with longitude −11°, visible over 50% of the orbit. There were 5 faint phase photons in 3221 s of exposure, 20 bright phase photons in 3440 s, and one photon during eclipse, which must be background and is accordingly neglected. The count rates are therefore approximately 4.95 ± 1.3 counts per kilosecond and 0.95 ± 0.7 counts per kilosecond. Using Poisson counting statistics, we ruled out the possibility that these count rates are equal at the 99.92% level.

For assumed plasma temperatures of 5 to 15 keV the bolometric flux of the source during bright phase was about $2{-}5 \times 10^{-13}$ erg s^{-1} cm^{-2}. This is an order of magnitude lower than the intermediate state (3.86×10^{12} erg s^{-1} cm^{-2}) observed in Worpel & Schwope (2015) and implies an accretion rate of $\dot{M} = 1{-}2 \times 10^{-13} M_{\odot}$ yr^{-1} (see Eq. (6.10) of Warner 1995).

Some accretion emission must have been present during the faint phase, because the source was still visible then. An unabsorbed blackbody with the temperature of a typical WD primary (≲15 000 K, e.g. Ferrario et al. 2015) would not have been detectable by *Swift* over 3.2 ks, as we verified with the *fakeit* command of Xspec, nor can the faint phase emission originate from the red dwarf donor star, for the same reason.

3.4.2. *Swift* UVOT observations

The UVOT instrument (Roming et al. 2005) used the *UVW2* filter, which has a central wavelength of 1928 Å. It was operated in image mode, so no photon arrival time information is available. The source was obviously visible in all five subexposures. The UVOT fluxes, as found with the *uvotdetect* task, for the five subexposures are summarised in Table 5. Each has been broken up into time contributions from the bright, faint, and eclipse phases. The mean X-ray photon barycentre correction of 454.9 s was used to perform barycentre corrections for the UVOT subexposure start and end times.

The fluxes of the first four exposures are similar. However eclipses occurred during exposures three and four and at these times the flux should drop to almost zero The first exposure occurred entirely during the faint phase. This timing information suggests that the bright phase flux during Obs3 and Obs4 might be brighter than the Obs1 faint phase by ~30–50%.

4. Discussion

4.1. J0328

From multiple X-ray observations of J0328 we have found strong evidence that its accretion rate varies strongly on timescales of a few months. It appeared to brighten slightly between 2012 January and February, before dimming significantly in March and brightening again by June and July.

We found an accretion dip for X-rays and visual light for J0328, but it was not present in UV. It is the second source, after V808 Aur, to exhibit this phenomenon (Worpel & Schwope 2015). A strong wavelength dependence of the transparency of the accretion stream may provide clues regarding its structure and physical properties. We have constrained the inclination of J0328 to approximately $45° < i < 77°$.

We have measured a magnetic field strength of 39 ± 2 MG for J0328 at the primary accreting pole, based on the unique identification of cyclotron harmonics. This value is somewhat higher than the 33 MG previously measured by Szkody et al. (2007).

If this source had been emitting with the same luminosity and spectral shape during the RASS, it would have had a count rate of about 0.033 counts per second in the ROSAT 0.1−2.4 keV band. It would not have been bright enough to be listed in the ROSAT Bright Sources Catalogue (Voges et al. 1999), but would probably have been detectable in the Faint Sources Catalogue (Voges et al. 2000).

We investigated the possibility of a large unobserved soft excess in the very soft X-ray regime and found that such a spectral component cannot be excluded, but – if it exists – it can only be concealed in a small area of the parameter space with temperatures of less than about 25 eV and an emitting area of a few hundred kilometers in radius.

4.2. J1333

J1333 was in a faint state during the *XMM-Newton* observation. It has never been observed in a bright state in X-rays, but was discovered in the SDSS, where it displayed a prominent HeII 4686 Å emission line caused by EUV photoexcitation. The CRTS photometry suggests that this system spends most of its time accreting at a low rate with only brief and infrequent periods of high accretion. We obtained a mean X-ray flux of 2.75×10^{-14} erg s^{-1} cm^{-2} and a plasma temperature of about 4 keV, but were not able to detect any periodicity in its light curve in either X-rays or UV. Further observations of this period-gap source would be helpful. Its inclination is less than 76°.

4.3. J1730

The object J1730 was detected in the ROSAT All-Sky Survey (RASS) at an average count rate of 0.096 ± 0.016 s^{-1} during the total exposure of 472 s. This is about twice as bright as in our *XMM-Newton* observation, indicating that its X-ray luminosity can vary significantly. The hardness ratios HR1 and HR2 of J1730 are compared to other white dwarf accretors, mostly cataclysmic binaries, in the ROSAT Bright Survey (RBS, Schwope et al. 2000) in Fig. 14. J1730 is found in a region occupied otherwise by non-magnetic CVs (dwarf novae and nova-likes) or by intermediate polars. These sources display mainly thermal spectra and the RASS X-ray colours of J1730 are indeed compatible with a thermal spectrum with $kT > 5$ keV absorbed by cold interstellar matter with $N_H \simeq 2 \times 10^{20}$ cm^{-2}. In particular they are lacking the soft component shown by the majority of RASS-discovered or RASS-observed polars. Only 2 among 23 RBS-polars showed hardness ratios compatible with thermal spectra, IW Eri and CD Ind (RBS541 and RBS1735), although with a significantly lower absorbing column density. The underlying population will be uncovered by upcoming sensitive surveys with e.g. eROSITA (Merloni et al. 2012).

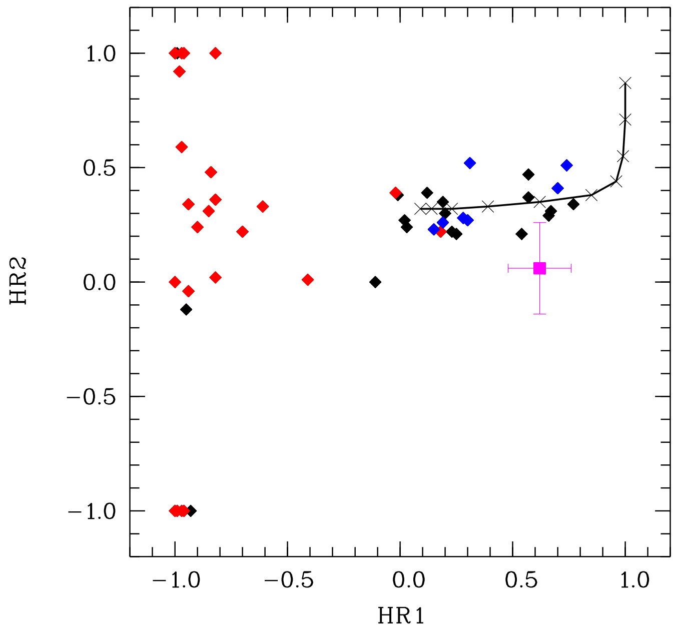

Fig. 14. X-ray colour-colour diagram of white dwarf accretors in the RBS (black – non-magnetic objects; blue – intermediate polars; red – polars). The location of J1730 is shown with error bars. The black line delineates a thermal spectrum with 10 keV absorbed by cold interstellar matter. Log N_H varies between 19 and 22 in steps of 0.33 dex, increasing from left to right.

The inclination of J1730 is not well constrained because there is no obvious accretion dip, but because of the lack of eclipses it is definitely less than 76° and probably less than 63°.

4.4. V808 Aur

We have revised the estimated distance to this source downwards, to about 250 pc. The analysis of the V808 Aur *Swift* observation completes the X-ray and UV characterisation of the source begun in Worpel & Schwope (2015). According to the light curve presented in Fig. 1 of Schwope et al. (2015) this observation occurred during the decline to a short low accretion state between two high states. In X-rays the star was about an order of magnitude fainter than in an intermediate phase observed in 2012 by *XMM-Newton* (Worpel & Schwope 2015), but easily detectable in both wavelength regimes.

There is a strong ($\gtrsim 3.3\sigma$) indication of a phase-dependent brightness variation. The bright phase, as defined by the ephemeris of the star and a sensible estimate of the accreting pole's location, is three times brighter than the faint phase. This result hints that an accreting pole is active and distinct even at this low $\dot{M}$. The source is detectable in the faint phase, suggesting some luminosity beyond the thermal emission of the white dwarf itself. We could not characterise the spectral differences between the bright and faint phases because not enough photons were detected. The bright phase in UV might be brighter than the faint phase by ~30−50% but the lack of timing information makes this difficult to determine.

The X-ray emission during the faint phase cannot be attributed to the companion star, or easily to a thermally emitting white dwarf surface. Accretion onto the distant hemisphere is a possible explanation but this hypothesis presents difficulties. As pointed out by e.g. Ferrario et al. (1989), transfer of material onto the distant pole is more likely at higher accretion rates. For low $\dot{M}$ the accretion stream is less dense and is captured by magnetic field lines further from the primary. The field lines taking the gas to the distant pole often protrude outside the Roche lobe of the primary, and it is energetically unfeasible for the gas to take this path. However, the wind-accreting pre-polars WX LMi (Schwarz et al. 2001) and HS0922+1333 (Reimers & Hagen 2000) show two-pole accretion geometry at very low accretion rate, demonstrating that a feasible trajectory to the second pole exists for some low accretion strongly magnetic CV systems.

For the crude MEKAL approximation to the count rate developed in Sect. 3.4.1, the ROSAT count rate would have been about 0.01 c/s. The sky position of V808 Aur was viewed by ROSAT for a total of 192 s in several scans separated by 96 min. Even if ROSAT had been able to observe the bright phase each time, this still would not have been enough to detect V808 Aur even in the ROSAT faint source catalogue (Voges et al. 2000). The non-detection of V808 Aur in ROSAT is therefore consistent with an accretion state similar to this one.

4.5. General remarks

The dichotomy between polars discovered in the *XMM-Newton* era, which all lack a prominent soft excess, and those identified as polars earlier, which all have it, can still only partly be explained. Polars lacking this feature may have been detectable in the 0.1−2.4 keV ROSAT band but would appear as unremarkable faint sources lacking amy distinguishing characteristics to motivate follow-up observations. This is probably true even of polars such as V808 Aur and J1730 which require a modest addition of flux below 2.0 keV to fit the *XMM-Newton* spectra. Thus, their pre-*XMM-Newton* non-discovery is unsurprising.

The other question, why there have been no discoveries of soft excess polars in the *XMM-Newton* era, remains unsolved. It cannot be purely due to the lack of a post-RASS all sky X-ray survey because polars can be discovered by *XMM-Newton* serendipitously (Vogel et al. 2008; Ramsay et al. 2009) or in optical surveys such as the SDSS. None of these have shown a soft excess. The upcoming eROSITA all-sky survey may uncover new objects of this kind, or provide insights as to why they might be missing.

It may be that in these systems the missing soft excess is actually present but so cool that it is outside *XMM-Newton*'s detection band. Our work (this paper and Worpel & Schwope 2015) has consistently shown that a blackbody-like component, up to 50−100 times more luminous than the plasma component, can be concealed in the extreme UV where it is invisible to *XMM-Newton*'s X-ray and optical telescopes. The current lack of a satellite sensitive in this energy range makes testing this hypothesis difficult.

Acknowledgements. This work was supported by the German DLR under contract 50 OR 1405. This work has made use of the Catalina Sky Survey. This study is based partly on data obtained with the STELLA robotic telescope in Tenerife, an AIP facility operated jointly by AIP and IAC. This research made use of Astropy (Astropy Collaboration et al. 2013) and the PARI-GP (PARI Group 2014) computer algebra package. Funding for the Sloan Digital Sky Survey IV has been provided by the Alfred P. Sloan Foundation, the US Department of Energy Office of Science, and the Participating Institutions. SDSS-IV acknowledges support and resources from the Center for High-Performance Computing at the University of Utah. The SDSS web site is `www.sdss.org`. SDSS-IV is managed by the Astrophysical Research Consortium for the Participating Institutions of the SDSS Collaboration including the Brazilian Participation Group, the Carnegie Institution for Science, Carnegie Mellon University, the Chilean Participation Group, the French Participation Group, Harvard-Smithsonian Center for Astrophysics, Instituto de Astrofísica de Canarias, The Johns Hopkins University, Kavli Institute for the Physics and Mathematics of the Universe (IPMU)/University of Tokyo, Lawrence Berkeley National Laboratory, Leibniz Institut für Astrophysik Potsdam (AIP), Max-Planck-Institut für Astronomie (MPIA Heidelberg), Max-Planck-Institut für Astrophysik (MPA Garching), Max-Planck-Institut für Extraterrestrische Physik (MPE), National Astronomical Observatory of China, New Mexico State University, New York University, University of Notre Dame, Observatário Nacional/MCTI, The Ohio State University, Pennsylvania State University, Shanghai Astronomical Observatory, United Kingdom Participation Group, Universidad Nacional Autónoma de México, University of Arizona, University of Colorado Boulder, University of Oxford, University of Portsmouth, University of Utah, University of Virginia, University of Washington, University of Wisconsin, Vanderbilt University, and Yale University.

References

Arnaud, K. A. 1996, in Astronomical Data Analysis Software and Systems V, eds. G. H. Jacoby, & J. Barnes, ASP Conf. Ser., 101, 17
Astropy Collaboration, Robitaille, T. P., Tollerud, E. J., et al. 2013, A&A, 558, A33
Beuermann, K. 2006, A&A, 460, 783
Bhalerao, V. B., van Kerkwijk, M. H., Harrison, F. A., et al. 2010, ApJ, 721, 412
Blackburn, J. K. 1995, in Astronomical Data Analysis Software and Systems IV, eds. R. A. Shaw, H. E. Payne, & J. J. E. Hayes, ASP Conf. Ser., 77, 367
Burrows, D. N., Hill, J. E., Nousek, J. A., et al. 2005, Space Sci. Rev., 120, 165
Chanan, G. A., Middleditch, J., & Nelson, J. E. 1976, ApJ, 208, 512
Churazov, E., Gilfanov, M., Forman, W., & Jones, C. 1996, ApJ, 471, 673
Coppejans, D. L., Körding, E. G., Knigge, C., et al. 2016, MNRAS, 456, 4441
Cropper, M. 1990, Space Sci. Rev., 54, 195
den Herder, J. W., Brinkman, A. C., Kahn, S. M., et al. 2001, A&A, 365, L7
Denisenko, D. V., & Korotkiy, S. 2009, vsnet-alert, 10870, 1
Denisenko, D. V., Kryachko, T. V., & Satovskiy, B. L. 2009, ATel, 2014, 1
Drake, A. J., Djorgovski, S. G., Mahabal, A., et al. 2009, ApJ, 696, 870
Eastman, J., Siverd, R., & Gaudi, B. S. 2010, PASP, 122, 935
Eisenstein, D. J., Weinberg, D. H., Agol, E., et al. 2011, AJ, 142, 72
Ferrario, L., Tuohy, I. R., & Wickramasinghe, D. T. 1989, ApJ, 341, 327
Ferrario, L., de Martino, D., & Gänsicke, B. T. 2015, Space Sci. Rev., 191, 111
Granzer, T., Weber, M., & Strassmeier, K. G. 2001, Astron. Nachr., 322, 295
Helene, O. 1983, Nucl. Instr. Meth. Phys. Research, 212, 319
Katysheva, N., & Shugarov, S. 2012, Mem. Soc. Astron. It., 83, 670
Kazarovets, E. V., Samus, N. N., Durlevich, O. V., Kireeva, N. N., & Pastukhova, E. N. 2015, IBVS, 6151
Kirsch, M. G. F., Altieri, B., Chen, B., et al. 2004, in UV and Gamma-Ray Space Telescope Systems, eds. G. Hasinger, & M. J. L. Turner, SPIE Conf. Ser., 5488, 103
Knigge, C. 2006, MNRAS, 373, 484
Kraft, R. P., Burrows, D. N., & Nousek, J. A. 1991, ApJ, 374, 344
Kuijpers, J., & Pringle, J. E. 1982, A&A, 114, L4
Liedahl, D. A., Osterheld, A. L., & Goldstein, W. H. 1995, ApJ, 438, L115
Lumb, D. H., Warwick, R. S., Page, M., & De Luca, A. 2002, A&A, 389, 93
Mason, K. O., Breeveld, A., Much, R., et al. 2001, A&A, 365, L36
Merloni, A., Predehl, P., Becker, W., et al. 2012, ArXiv e-prints [arXiv:1209.3114]
Mewe, R., Gronenschild, E. H. B. M., & van den Oord, G. H. J. 1985, A&AS, 62, 197
PARI Group 2014, PARI/GP version 2.7.0, Bordeaux, http://pari.math.u-bordeaux.fr/
Ramsay, G., & Cropper, M. 2004, MNRAS, 347, 497
Ramsay, G., Rosen, S., Hakala, P., & Barclay, T. 2009, MNRAS, 395, 416
Reimers, D., & Hagen, H.-J. 2000, A&A, 358, L45
Revnivtsev, M., Sazonov, S., Krivonos, R., Ritter, H., & Sunyaev, R. 2008, A&A, 489, 1121

Roming, P. W. A., Kennedy, T. E., Mason, K. O., et al. 2005, Space Sci. Rev., 120, 95
Saxton, R. D., Read, A. M., Esquej, P., et al. 2008, A&A, 480, 611
Schmidt, G. D., Szkody, P., Vanlandingham, K. M., et al. 2005, ApJ, 630, 1037
Schmidt, G. D., Smith, P. S., Szkody, P., & Anderson, S. F. 2008, PASP, 120, 160
Schwarz, R., Schwope, A. D., & Staude, A. 2001, A&A, 374, 189
Schwarzenberg-Czerny, A. 1989, MNRAS, 241, 153
Schwope, A. D., & Beuermann, K. 1990, A&A, 238, 173
Schwope, A. D., Beuermann, K., Jordan, S., & Thomas, H.-C. 1993, A&A, 278, 487
Schwope, A., Hasinger, G., Lehmann, I., et al. 2000, Astron. Nachr., 321, 1
Schwope, A. D., Mackebrandt, F., Thinius, B. D., et al. 2015, Astron. Nachr., 336, 115
Shevchuk, A. S., Fox, D. B., Turner, M., & Rutledge, R. E. 2009, ATel, 2015, 1
Southworth, J., Tappert, C., Gänsicke, B. T., & Copperwheat, C. M. 2015, A&A, 573, A61
Strassmeier, K. G., Granzer, T., Weber, M., et al. 2004, Astron. Nachr., 325, 527
Strüder, L., Briel, U., Dennerl, K., et al. 2001, A&A, 365, L18
Szkody, P., Henden, A., Mannikko, L., et al. 2007, AJ, 134, 185
Szkody, P., Anderson, S. F., Hayden, M., et al. 2009, AJ, 137, 4011
Templeton, M., Oksanen, A., Boyd, D., Pickard, R., & Maehara, H. 2009, Central Bureau Electronic Telegrams, 1652, 1
Thomas, H.-C., Beuermann, K., Burwitz, V., Reinsch, K., & Schwope, A. D. 2000, A&A, 353, 646
Thorne, K., Garnavich, P., & Mohrig, K. 2010, IBVS, 5923, 1
Turner, M. J. L., Abbey, A., Arnaud, M., et al. 2001, A&A, 365, L27
Vogel, J., Byckling, K., Schwope, A., et al. 2008, A&A, 485, 787
Voges, W., Aschenbach, B., Boller, T., et al. 1999, A&A, 349, 389
Voges, W., Aschenbach, B., Boller, T., et al. 2000, IAU Circ., 7432, 3
Warmels, R. H. 1992, in Astronomical Data Analysis Software and Systems I, eds. D. M. Worrall, C. Biemesderfer, & J. Barnes, ASP Conf. Ser., 25, 115
Warner, B. 1995, Cambridge Astrophys. Ser., 28
Worpel, H., & Schwope, A. D. 2015, A&A, 583, A130